Constraints for the martian crust structure from Rayleigh waves ellipticity of large seismic events

Sebastián Carrasco[1], Brigitte Knapmeyer-Endrun[1], Ludovic Margerin[2], Zongbo Xu[3], Rakshit Joshi[4], Martin Schimmel[5], Eleonore Stutzmann[3], Constantinos Charalambous[6], Philippe Lognonné[3], W. Bruce Banerdt[7]

[1]Bensberg Observatory, University of Cologne, Bergisch Gladbach, Germany
[2]Institut de Recherche en Astrophysique et Planétologie, Université Toulouse III Paul Sabatier, CNRS, CNES, Toulouse, France
[3]Université Paris Cité, Institut de physique du globe de Paris, CNRS, Paris, France
[4]Max Planck Institute for Solar System Research, Göttingen, Germany.
[5]Geosciences Barcelona, CSIC, Barcelona, Spain.
[6]Department of Electrical and Electronic Engineering, Imperial College London, South Kensington Campus, London, United Kingdom
[7]Jet Propulsion Laboratory, California Institute of Technology, Pasadena, CA 91109, USA

Key Points:

- Rayleigh waves ellipticity was measured at long periods (15-35 s) at the InSight landing site using large seismic events, including S1222a.
- A 4-layer crust model, including a shallow low-velocity layer, explains the local-scale observations.
- Low crustal velocities are derived for the InSight site, which may be due to high porosity or heavy alteration at local scale.

Corresponding author: Sebastián Carrasco, acarrasc@uni-koeln.de

Abstract

For the first time, we measured the ellipticity of direct Rayleigh waves at long periods (15 - 35 s) on Mars using the recordings of three large seismic martian events, including S1222a, the largest event recorded by the InSight mission. These measurements, together with P-to-s receiver functions and P-wave reflection times, were utilized for performing a joint inversion of the local crust structure at the InSight landing site. Our inversion results are compatible with previously reported intra-crustal discontinuities around 10 and 20 km depths, whereas the preferred resulting models show a strong discontinuity at ∼37 km, which is interpreted as the crust-mantle interface. We propose the presence of a top shallow low-velocity layer of 2-3 km thickness. Compared to nearby regions, lower seismic wave velocities are derived for the local crust, thus suggesting a higher porosity or alteration of the whole local crust.

Plain Language Summary

As never before on Mars, we measured the characteristics of the seismic waves traveling along the martian surface that carry information about the crust structure at the InSight site. We combined these measurements with two other local-scale independent observations to derive a consolidated model for the crust underneath the InSight lander. Our results suggest a martian crust with 4 layers and, particularly, one thin layer of about 2 km thickness close to the surface. The crust-mantle discontinuity was found at ∼37 km depth, where the sharpest change in seismic wave velocity is observed. Overall, the seismic wave velocities of the local martian crust at the InSight site are lower than those derived in other regions on Mars, which suggest a higher porosity or local alteration.

1 Introduction

The structure and properties of the martian crust are important for understanding the evolution of Mars and rocky planets. In this context, the InSight mission (Banerdt et al., 2020), which landed on Elysium Planitia in November 2018, aims to study the interior of Mars by means of one seismological station placed on the martian surface (Lognonné et al., 2019).

After more than three years of InSight data collection, the martian crust has been studied by a thorough analysis of the InSight seismological data. In particular, early analysis of P-to-s receiver functions (RFs) allowed to derive a shallow layer with low seismic velocities in the first 8-11 km of the martian crust at the landing site (Lognonné et al., 2020). Further investigation including more marsquakes suggests a layered martian crust beneath the InSight lander with two discontinuities at 8 ± 2 km and 20 ± 5 km, and a bimodal estimation of the crust thickness of either 20 ± 5 or 39 ± 8 km (Knapmeyer-Endrun et al., 2021). Lately, the analysis of further seismic events and the identification of other secondary phases (PPs, Sp and three new crustal multiples) favor a 3-layer crustal model (Kim et al., 2021; Joshi et al., 2023; Durán et al., 2022), for which the crust-mantle boundary would be located at ~ 40 km depth. The shallow discontinuity around 8 km depth has been confirmed by the detection of SsPp phases (J. Li, Beghein, Davis, et al., 2022) and SH-wave reflections (J. Li, Beghein, Wookey, et al., 2022). Besides, the identification of both PP and SS precursors indicates that the second discontinuity observed at the InSight site (at ~ 20 km depth) is also present around 4000 km away from the station and has been interpreted as a regional or global feature (J. Li, Beghein, McLennan, et al., 2022). On a global scale, Wieczorek et al. (2022) have estimated an average thickness of the martian crust between 30 and 72 km and a maximum permissible crustal density between 2850 and 3100 kg m^{-3}. Further properties and characteristics of the martian crust at regional scales have been derived from the analysis of the InSight seismic data using different approaches (e.g., Kim, Banerdt, et al., 2022; Beghein et al., 2022; Kim, Stähler, et al., 2022; J. Li, Beghein, Lognonné, et al., 2022). Nevertheless, the el-

lipticity analysis of direct Rayleigh waves is still a pending task that could provide further constraints on the structure of the martian crust at the InSight landing site, as proposed by Panning et al. (2017).

Besides RFs, the analysis and inversion of the ellipticity of direct Rayleigh waves is a single-station technique that, when measured at long periods (>10 s), allows investigating the local underground structure down to crustal depths (Tanimoto & Rivera, 2008; Yano et al., 2009). In this sense, the ellipticity has been shown to be invariant to the seismic source, the wave propagation path or the epicentral distance and rather depend on the local structure directly beneath the receiver site (e.g., Ferreira & Woodhouse, 2007). Even though this methodology was proposed in the 1970s, it has gained popularity only in recent years and with successful applications on Earth (e.g., Lin et al., 2012; G. Li et al., 2016; Berbellini et al., 2017), but it has not been applied on Mars so far due to the lack of observation of direct Rayleigh waves and, therefore, the characteristic ellipticity of the InSight site at long periods remains unknown.

On May 4, 2022, the InSight lander recorded the S1222a event, which had a moment magnitude estimated as M_W 4.7 and thus corresponds to the largest seismic event ever recorded on Mars (Kawamura et al., 2022). This event exhibits clear surface waves (both Love and Rayleigh) that can be used for studying lithosphere properties along the source-receiver path (e.g., Beghein et al., 2022; J. Li, Beghein, Lognonné, et al., 2022; Kim, Stähler, et al., 2022), but is also a unique opportunity to investigate the local crust structure through ellipticity analysis of Rayleigh waves. Similarly, the events S1000a and S1094b are two other good quality seismic events caused by the impact of meteorites on the martian surface (Posiolova et al., 2022), and for which Rayleigh waves have been observed (Kim, Banerdt, et al., 2022). These three large events are thus excellent candidates to perform a Rayleigh waves ellipticity (also referred to as ε) analysis.

The analysis of ε data can be used as an independent observation to characterize the martian crust at the InSight landing site. In fact, even though the inversion of ε data-only can be performed to map the mechanical properties (especially shear-wave velocity, V_s) of the local subsurface, there is a great non-uniqueness of the solutions. In a similar way, the inversion of RFs is affected by the non-uniqueness phenomenon and, although this observation is highly sensitive to discontinuities, the addition of ε data can provide constraints to long-wavelength velocity features (Chong et al., 2016). As both data sets map the local structure at similar local scales, a joint inversion of ε and P-to-s RFs data can be performed. Similarly, the autocorrelation times obtained from the analysis of seismic ambient noise, such as those by Schimmel et al. (2021), are sensitive to the local crustal structure and therefore can be used as an independent data set to constrain the inversion.

In this work, we analyze the ellipticity and phase shift of the Rayleigh waves related to the large seismic events S1000a, S1094b and especially S1222a, to obtain further constraints on the structure of the Martian crust. In particular, we perform a joint inversion of Rayleigh wave ellipticity, P-to-s RFs and autocorrelation times, aiming to obtain a consolidated local crustal model.

2 Data processing and methods

2.1 Rayleigh wave ellipticity

In order to retrieve the characteristic ε at the InSight site, we performed a time-domain analysis in a similar way as has been performed on Earth (e.g., Ferreira & Woodhouse, 2007; Berbellini et al., 2016; Ferreira et al., 2020), following the steps shown in Fig. 1. First, the time windows where the Rayleigh waves arrive are roughly estimated by manual inspection, following the identification by Kim, Banerdt, et al. (2022) for S1000a and S1094b and the time estimates by the Marsquake Service (MQS) for S1222a (Kawa-

mura et al., 2022), and assuming they correspond to the fundamental mode ($_0R_1$). These arrival time windows are shown in Fig. 1a, where the arrival of a suspected first overtone of the Rayleigh wave ($_1R_1$) for S1222a is also outlined, but it is not used in this work due to the low amplitude of the signal on the radial component.

The raw data (InSight Mars SEIS Data Service, 2019) are restituted to ground motion (displacement) and transferred into the ZNE coordinates system. The data are then rotated into a ZRT coordinates system by using the back azimuth (BAZ) of each event. Particularly, as S1000a and S1094b have been identified as impacts with source locations confirmed by orbital images (Posiolova et al., 2022), their BAZs are well constrained at around 36° and 51°, respectively. For S1222a, even though there are estimates for the location of the source (e.g., Kawamura et al., 2022), there is no ground-truth location as for S1000a and S1094b. Accordingly, we applied an independent methodology to estimate the BAZ of S1222a, based on the analysis of the Rayleigh waves. Our estimate is based on the fact that the Rayleigh waves propagate in the ZR plane and, thus, we look for the maximization of the ground-motion amplitudes on the Z and R components while minimizing the ground motion on the T component. Further details on this methodology are provided in section S1 (Supp. Material). In the case of S1222a, our estimates for the BAZ are in the range 114°-137°, with a median value of 129°, which is used in this work. Our BAZ is in the range of back azimuths obtained from the analysis of multi-orbit Rayleigh waves (Panning et al., 2022) and differs by $\sim 30°$ from the BAZ derived from body waves by the MQS (Kawamura et al., 2022). This difference might be due to off-great-circle propagation of the Rayleigh waves, which is caused by strong lateral heterogeneities along the source-receiver path (Evernden, 1953; Ji et al., 2005), particularly because they likely travel along the Martian dichotomy (Panning et al., 2022; Kim, Stähler, et al., 2022). In this region, clear topographic differences are observed between the northern and southern hemispheres. After rotating into the ZRT coordinates system, the Z and R components are bandpass-filtered, with a 30% bandwidth, around different central periods T_0 (Fig. 1b). In this way, every T_0 will be associated with one ellipticity value.

Subsequently, we obtained the optimal phase shift (ϕ) by maximizing the cross-correlation between the Z and R components. Examples of resulting ϕ and optimally shifted waveforms are shown in Fig. 1c for the three events studied here. Once optimally shifted, we computed the cross-correlation factor $\nu(t)$, ranging from -1 to 1, between the shifted Z and R components (Fig. 1d). The normalized envelope ($\eta(t)$), also shown in Fig. 1d and given by the multiplication of the Z and R envelopes, is calculated in order to find the specific time window where the energy is maximized. In order to discard low-amplitude signals with high cross-correlation (or vice versa), a characteristic function $\chi(t) = \nu(t)\eta(t)$ is calculated (Fig. 1e). The final ellipticity for the central period T_0, computed as the R/Z quotient, corresponds to the average of the ellipticities in the time window where the characteristic function χ is larger than 0.8, as shown in Fig. 1f.

These processing steps are performed on the observed fundamental mode of the direct Rayleigh waves ($_0R_1$) of the events S1000a, S1094b and S1222a. In order to combine these measurements, even though radial and azimuthal anisotropy may be present, we consider that these would affect ellipticity to a lesser extent than the underlying crustal structure. One ε value is obtained for each event and each central period T_0. To get the characteristic ellipticity curve at the InSight landing site, only pairs of event-T_0 with actual Rayleigh wave signal are considered, which is achieved by choosing data time windows where the signal-to-noise ratio (SNR) is larger than a given threshold in both Z and R components. We use $\mathrm{SNR}_Z \geq 10$ and $\mathrm{SNR}_R \geq 5$ (given the higher noise levels on the horizontals). The final Rayleigh ellipticity curve for the InSight site is then calculated as the smoothed median of the valid ε values, obtained by means of a Savitzky-Golay filter (Savitzky & Golay, 1964).

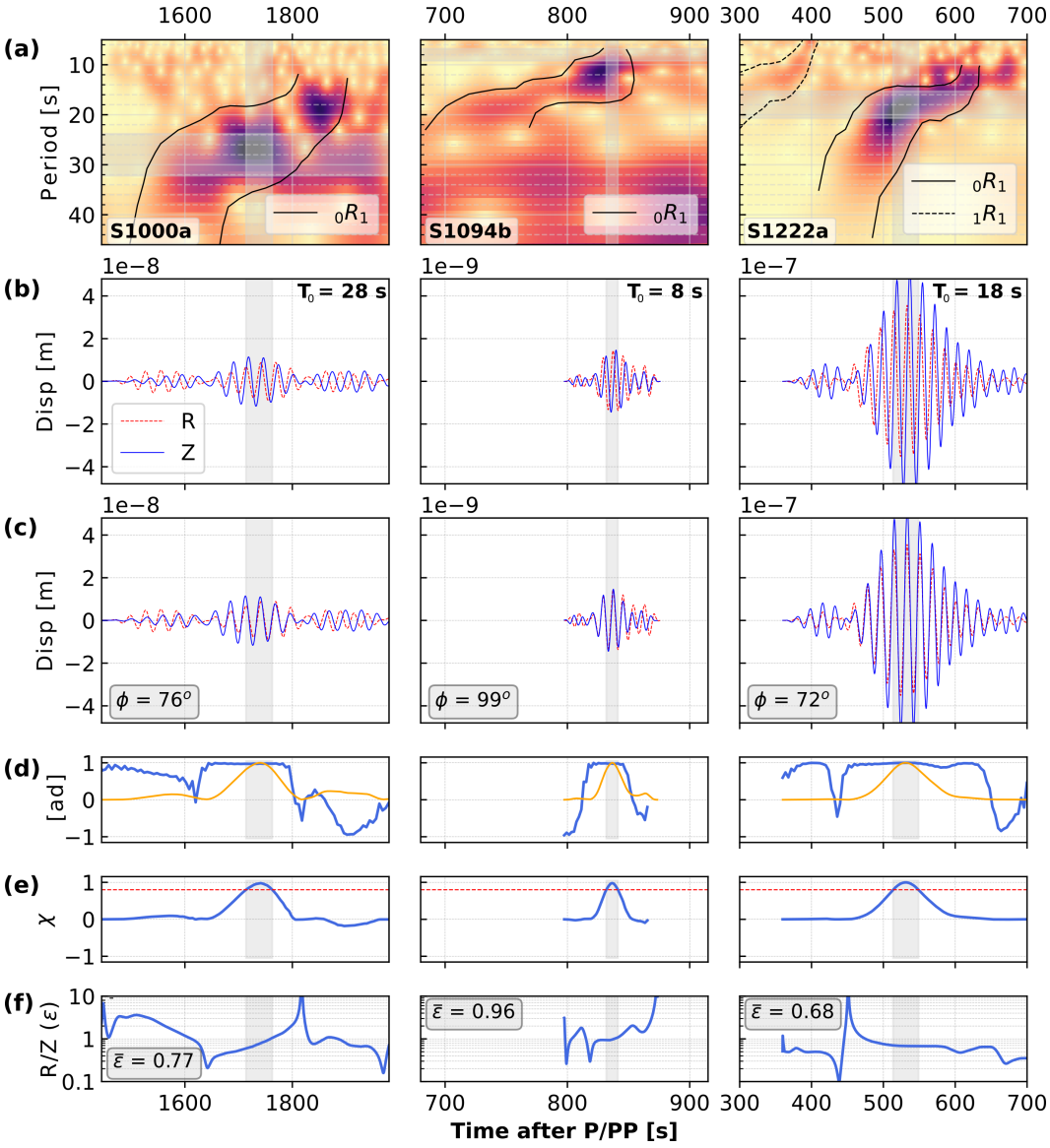

Figure 1. Extraction of Rayleigh wave ellipticity from large marsquakes. From left to right, columns correspond to events S1000a, S1094b and S1222a, respectively. From top to bottom: **(a)** S-transform spectrogram of the Z component, where the fundamental mode and first overtone of the Rayleigh waves are highlighted; **(b)** unshifted vertical (Z, solid blue) and radial (R, dashed red) components bandpass-filtered with a 30% bandwidth around a given central period T_0, where the Rayleigh wave is clearly visible for each event. The spectral range shown in each case is also denoted by the horizontal gray area in (a); **(c)** shifted Z and R waveforms using the optimal phase shift for the given period; **(d)** cross-correlation factor between shifted Z and R components (blue) and the envelope of ZR(t) (yellow); **(e)** characteristic function $\chi(t)$, where the red dashed line denotes a minimum threshold $\chi = 0.8$; **(f)** ellipticity $\varepsilon(t)$. For each event and each central period, the average ellipticity ($\bar{\varepsilon}$) is computed over the time window where $\chi \geq 0.8$ (gray box).

2.2 Joint inversion of ellipticity, P-to-s RFs and autocorrelation times

As the trade-off between the layer velocities and the depth of the discontinuities is a well-known feature of the ellipticity inversion, the incorporation of independent measurements such as receiver functions and autocorrelation times can help to further constrain the possible models (Chong et al., 2016). Because of this, we retrieved the 1D crustal structure underneath the InSight landing site by jointly inverting the ε measurements (this work) with the mean P-to-s RF by Joshi et al. (2023), which was obtained by stacking radial-component receiver functions for eight high-quality marsquakes mainly originating in the Cerberus Fossae region. Further details on the processing of the RF data can be found in Joshi et al. (2023). Additionally, we included the autocorrelation times obtained by Schimmel et al. (2021), which are understood as the two-way travel times of P waves bouncing back from the first ($\sim$ 6.15 s) and second ($\sim$ 10.6 s) strong discontinuity within the crust.

For every model, the RF forward calculation is performed via a Python implementation of the code by Shibutani et al. (1996), using a fixed ray parameter $p^* = 6.9$ s/deg, suitable for events in the Cerberus Fossae region (Joshi et al., 2023). In the RF, four peaks at around 0, 2.4, 4.8 and 7.2 s are observed, which are related to the direct P phase and three converted phases P_1s, P_2s, P_3s, where the subscript indicates the interface where each phase is generated. The synthetic ellipticity curves are obtained via the *gpell* toolbox included in the Geopsy package (Wathelet, 2005). Lastly, the autocorrelation times are computed assuming two-way vertical travel paths of the P waves.

The inversion scheme utilized is the Neighbourhood Algorithm (NA), first introduced by Sambridge (1999), that has been widely used for multiple geophysical applications and, particularly, for subsurface characterization (e.g., Hobiger et al., 2013; Ferreira et al., 2020; Carrasco et al., 2022). We applied a modified version of the NA, where the parameters space can be constrained by physical conditions and prior information (Wathelet, 2008). Among other constraints, we used the main outcomes of the transdimensional inversion of P-to-s RFs by Joshi et al. (2023), who found confirmation for a 3-layer crust model and provide constraints for the depths of the largest discontinuities. The NA is based on a fully non-linear, self-adaptive Monte Carlo approach, which efficiently explores the parameters space in order to find the model $\mathbf{m}$ that minimizes the misfit function Ψ between the observed and theoretical data. For each explored model $\mathbf{m}$, Ψ is defined as:

$$\Psi(\mathbf{m}) = W_e\psi_e(\mathbf{m}) + W_{rf}\psi_{rf}(\mathbf{m}) + W_a\psi_a(\mathbf{m}), \tag{1}$$

where the weights of the ellipticity (W_e), the receiver functions (W_{rf}) and autocorrelation times (W_a) data sets were fixed to 0.45, 0.45 and 0.1, respectively, to explain mainly the ε and RFs measurements, with a small constraint given by the autocorrelation times. The $\psi_i(\mathbf{m})$ terms correspond to the individual misfits of each data set, given by the fit between the observed and synthetic calculations for each model $\mathbf{m}$. Further details can be found in section S6 (Supp. Material).

3 Results and discussion

3.1 Ellipticity and phase-shift observations

The resulting ε and ϕ values are shown in Fig. 2a and b, respectively. Besides the limited number of events analyzed, there is a lack of valid ellipticity measurements due to the low-amplitude energy on the radial component.

The valid ε values, i.e., those for which the imposed SNR criteria are fulfilled, define an ellipticity curve between 15 and 35 s and two points at 8 and 9 s (Fig. 2). For

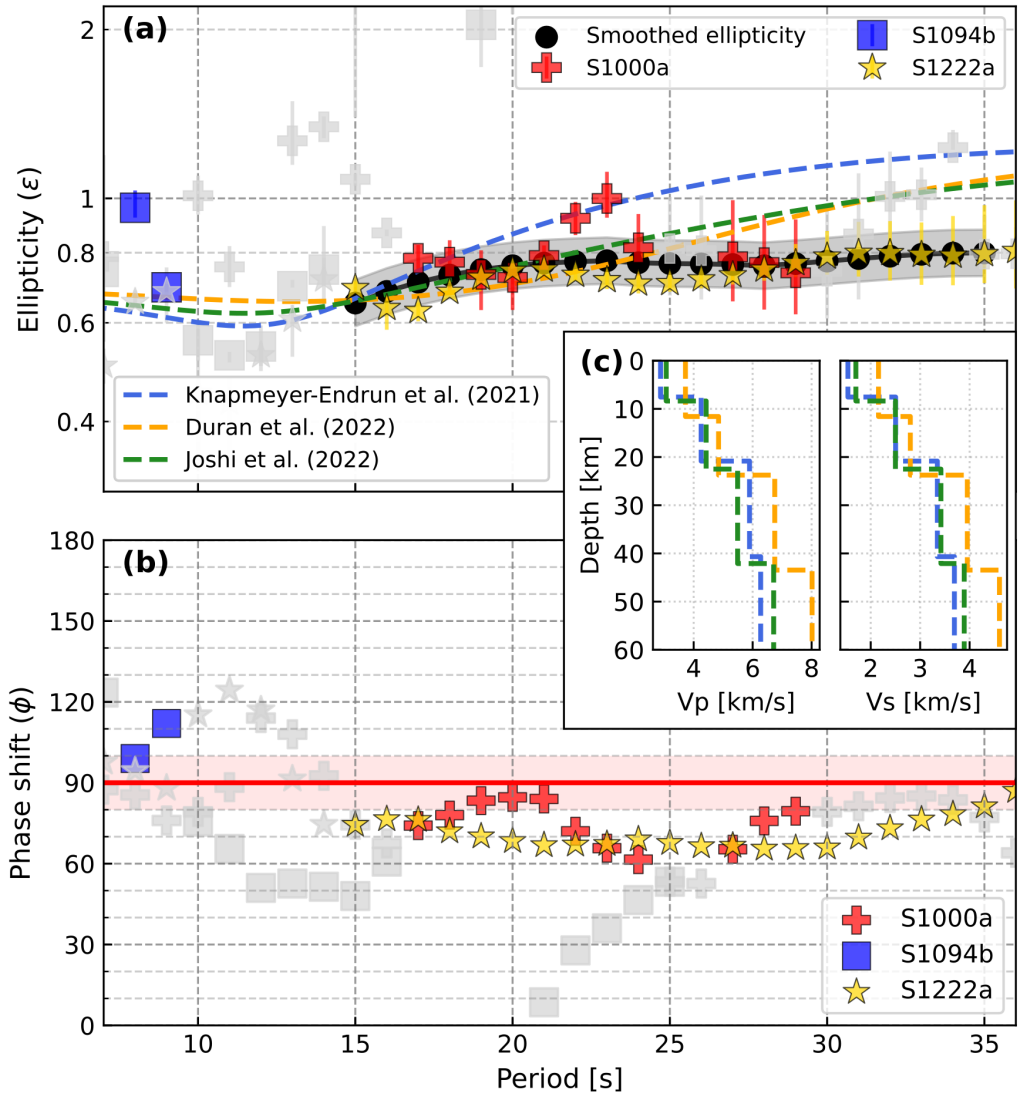

Figure 2. Rayleigh wave ellipticity and phase shift results. **(a)** Rayleigh wave ellipticity (ε) retrieved at different central periods T_0 for the three large events S1000a (red cross), S1094b (blue square) and S1222a (yellow star). Colored markers correspond to periods where the SNR criteria are fulfilled. Background light gray markers did not meet the minimum SNR threshold. The final ellipticity curve for the InSight site is denoted by the black circles, and a 15% uncertainty range has been imposed (gray area). Synthetic ellipticity curves are illustrated for characteristic crustal models from Knapmeyer-Endrun et al. (2021), Durán et al. (2022) and Joshi et al. (2023). **(b)** Phase shift ϕ between Z and R components of ${}_0R_1$ for the same events and with the same color code as in (a). The light red area corresponds to ϕ in the range 90±10°. **(c)** Vp and Vs models for the InSight crust used for synthetic calculation of Rayleigh wave ellipticity in (a).

the purpose of this paper, we will focus on the period range between 15 and 35 s. In this range, the horizontal contribution of the tilt induced by Rayleigh waves can be neglected. Due to the lack of further observations, a common 15% uncertainty is utilized, which properly covers our observations. The resulting ellipticity curve is rather flat, especially between 20 and 35 s, with a slight decrease towards shorter periods. No strong peaks or troughs are observed in this period range.

On Earth, the ellipticity curve of one specific site is obtained from the recordings of a large number of earthquakes. In our work, even though three events were initially investigated, the ellipticity curve is mainly ruled by S1222a and therefore the lack of observations can be disadvantageous for further analysis and interpretation. It has been shown that ellipticity data can have a large spread (Berbellini et al., 2016; Attanayake et al., 2017), which has been associated with complex Rayleigh wave propagation effects (Sexton et al., 1977; Pedersen et al., 2015).

For a better assessment, the same ellipticity analysis was performed for one station on Earth (station BQ.DREG in Germany, see section S2 in Supp. Material). These measurements suggest that well-recorded events can show some variation with respect to the characteristic smoothed ellipticity curve of the site, but the broad shape of the curve remains similar. In particular, some events show different slopes and trends at specific period ranges, with respect to what is observed for the median ellipticity (Fig. S2 and S3), but the general trend is the same. Thus, we conclude that small oscillations on the ellipticity curve should not be over-interpreted. It is also worth noting that the uncertainty range of these Earth observations is about 20%, close to the error range utilized here. Besides, in the InSight case, the ${}_0R_1$ of the event S1222a has a high SNR in both Z and R components, so the final smoothed ε is expected to be a good representation of the local structure.

We calculated synthetic ellipticity values for representative three-layer crust models (see section S4), based on the inversion results by Knapmeyer-Endrun et al. (2021), Durán et al. (2022) and Joshi et al. (2023). These models were derived from the inversion of P-to-s RFs from different sets of martian seismic events and, in the case of Joshi et al. (2023), combined with apparent S-wave velocities, whereas Durán et al. (2022) also included teleseismic data. Even though the corresponding ellipticity curves have a good fitting at periods between 15 and 21 s, all these models overestimate ε at longer periods (Fig. 2a). Furthermore, the calculated times of the P-wave reflections for these models (Table S1) do not fit the times from the seismic noise autocorrelations analysis (Schimmel et al., 2021), which further encourages a joint inversion of the three data sets.

Besides the ellipticity values, the resulting Z-R phase shifts are another interesting observation. Mainly ruled by the S1222a event, our results suggest ϕ values between 60° and 70° (Fig. 2b), which are persistently lower than the theoretical phase shift for Rayleigh waves under isotropic and homogeneous conditions (90°). Considering the possible uncertainties, we tested different values of back azimuth for S1222a and the resulting ϕ are still persistently lower than 90° (see Fig. S5).

On Earth, variations of ϕ are usually in the range 80-100°, but larger deviations up to ±30° have been also found and have been proposed to be related to small-scale heterogeneities (e.g., Ferreira & Woodhouse, 2007). This phenomenon has been less well-studied than ellipticity, so the interpretation of this observation is challenging. According to our observations on Earth for station DREG, even though a typical 90° phase shift is measured for most of the earthquakes, low ϕ ($60-75°$) were measured for some earthquakes at specific period ranges (see Fig. S4). These observations suggest that anomalous ϕ might be related to the Rayleigh-waves path, or even the source, rather than the characteristics of the receiver site. However, Tanuma & Man (2008) also proposed that variations of ϕ with respect to the isotropic theoretical value depend on the perturbation of the initial stress conditions of the medium. Under these considerations, the low

ϕ measured at the InSight landing site might be due to a combination of path or source effects with the initial stress conditions at this site, but not directly related to the mechanical characteristics of the crust at the InSight landing site. In any case, low ϕ values have previously been observed on Earth to occur in some cases. Further analysis of this phenomenon is beyond the scope of this work.

3.2 Local crust structure at the InSight landing site

In order to derive a consolidated crustal structure for the InSight landing site, the joint-inversion of the ellipticity measurements (this work), P-to-s RFs (Joshi et al., 2023) and P-wave reflection times (Schimmel et al., 2021) was performed. In this regard, it is worth noting that the inversion of ellipticity data alone does not properly constrain the local crustal structure. In fact, the ellipticity inversion using different settings between one and four layers over a half-space can equally well explain the ε observations (Fig. S6).

The initial joint-inversion results suggest that these local measurements can be well explained by a three-layer model, with an overall good fitting of the three data sets (see Fig. S8). However, the amplitude of the P-phase (first peak on the RFs), which is not normalized as it provides information on the near-surface velocities (e.g., Ammon, 1991), is clearly overestimated. As shown by synthetic forward modeling (Fig. S9), lower amplitudes for this arrival can be achieved by having lower velocities in the first layer. Because of this, we performed a second inversion where we allowed a shallow low-velocity layer (see Table S3 for details on the parameter space).

The resulting models from this second inversion are preferred as they explain the three independent data sets reasonably well (Fig. 3a-d), and especially the amplitude of the direct P-phase arrival is well retrieved. The predicted ellipticity curves have a better fitting at long periods (between 25 and 35 s) than between 15 and 25 s, where the short-scale curvature cannot be fully modeled (Fig. 3a). This slight discrepancy may be related to the lack of data for proper averaging and smoothing of the ellipticity curve, as can be done on Earth (e.g., Fig. S2). As discussed above, we consider the long-wavelength shape of the ellipticity curve to be the most reliable observation and, therefore, our inversion results provide an acceptable prediction of it. On the other hand, the autocorrelation times are well predicted within their uncertainty range (Fig. 3b).

The arrival times and amplitudes of the main phases on the RF are also well predicted by our best-resulting models (Fig. 3b), but some discrepancies are observed for the amplitude of the second peak ($\sim$ 2.2 s). This mismatch can be related to a larger amplitude variability of the P_1s phase (see Fig. 3 in Joshi et al., 2023). In any case, the two arrival times and the amplitudes of the major peaks are well retrieved.

Our preferred models show that the crust at the InSight landing site can be understood as a four-layer crust, including a shallow low-velocity layer (sLVL) close to the surface. The sLVL presents low velocities between 1.5 and 1.8 km/s and extends down to 2-3 km depth. Its origin is unclear, but previous works on the shallowest structure of Mars have proposed the presence of sedimentary and heavily fractured basalt layers in the first hundreds of meters (Hobiger et al., 2021; Carrasco et al., 2022), where shear-wave velocities below 1 km/s were derived. Furthermore, Pan et al. (2020) suggested the presence of a sedimentary layer extending from 200-300 m up to kilometers in depth, whereas Warner et al. (2022) showed evidence for heavily fractured basalt units in the surrounding area. Thus, we interpret this shallow discontinuity to be the end of this large-scale either sedimentary or heavily fractured basalt layer. A similar observation of such a shallow layer, based on the analysis of high-frequency RFs of S1222a, has been also recently proposed by Shi et al. (2022).

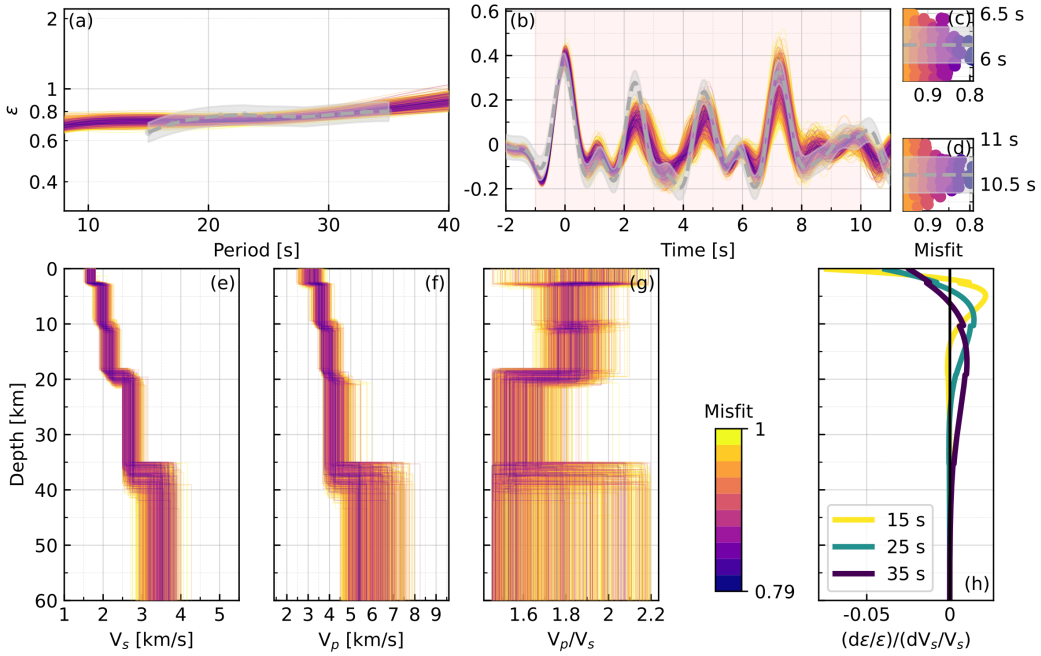

Figure 3. Joint-inversion results and resulting local martian crustal models. The measurements and the synthetic modeling of the 200 best-fitting crustal models are shown for **(a)** Rayleigh wave ellipticity, **(b)** P-to-s RFs from Joshi et al. (2023), and **(c)** first and **(d)** second P-wave reflection times by Schimmel et al. (2021). The light gray dashed line and area correspond to the measured data and their uncertainty, respectively, whereas the synthetic data are colored by their misfit. The corresponding crustal models are shown in terms of their **(e)** S-wave velocity V_s, **(f)** P-wave velocity V_p and **(g)** V_p/V_s, as a function of depth. **(h)** Depth sensitivity kernels for a characteristic resulting model calculated at three different periods: 15 s (yellow), 25 s (green) and 35 s (dark blue). Light red box in (b) shows the time window where the data was fitted.

Below this shallow layer, our models have a similar structure and the discontinuities at ~ 10 and ~ 20 km depth are in good agreement with previously reported models for the local crust (e.g., Knapmeyer-Endrun et al., 2021; Durán et al., 2022; Joshi et al., 2023). A third discontinuity is derived at around 37 km depth and it is interpreted as the crust-mantle boundary, where the sharpest velocity contrast is observed and where the ellipticity data has low sensitivity (Fig. 3h). Nevertheless, the ellipticity data can properly constrain the velocities at shallow depths and, given the identification of the P_3s phase on the RF, the joint-inversion can provide reliable depths for this discontinuity.

Our preferred models present overall P-wave and S-wave velocities lower than 5 and 3 km/s, respectively, for the whole crust. Particularly, the shear-wave velocities are lower than those in nearby regions on Mars. For example, Kim, Banerdt, et al. (2022) found V_s around 3.2 km/s, between 5 and 30 km depth, for a path between Amazonis Planitia and the InSight site, in the lowlands. Similarly, V_s between 3.05-3.17 km/s were derived for the upper crust (first 20 km) of the path between S1222a and the lander ($\sim$2190 km distance), along the dichotomy region (J. Li, Beghein, Lognonné, et al., 2022). At a local scale, our proposed shear-wave velocities are also lower than those previously reported for the InSight site (Knapmeyer-Endrun et al., 2021; Durán et al., 2022; Joshi et al., 2023). Therefore, following the crustal layering interpretation by Wieczorek et al. (2022), and considering that porosity plays an important role in decreasing the velocity of the seismic waves (e.g., Heap, 2019), these lower velocities might be related to an even larger porosity or stronger alteration of the whole crust at the InSight site.

4 Conclusions

For the first time, the ellipticity of the fundamental mode of direct Rayleigh waves was measured on Mars for long periods, especially thanks to S1222a: the largest event recorded on Mars so far. The obtained ellipticity curve, between 15 and 35 s, is a good representation of the characteristic ellipticity at the InSight landing site. Anomalously low phase shifts were measured, which seem to be unrelated to the local crust structure. In order to consolidate the local crustal model, we performed a joint inversion of local-scale observations (ellipticity, P-to-s RFs and P-wave reflection times). Our results suggest a four-layer crustal model, with a shallow low-velocity layer of about 2-3 km thickness at the InSight landing site. Other discontinuities around 10, 20 and 37 km depth correlate well with previously reported models. We propose lower P- and S-wave velocities for the corresponding crustal layers, which might be related to a higher porosity or alteration of the martian crust at the InSight landing site.

Acknowledgments

The authors acknowledge NASA, CNES, their partner agencies and institutions (UKSA, SSO, DLR, JPL, IPGP-CNRS, ETHZ, IC and MPS-MPG), and the flight operations team at JPL, SISMOC, MSDS, IRIS-DMC and PDS for providing SEED SEIS data. Thanks to Dr. J. Li for his thoughtful comments about the manuscript. French co-authors acknowledge the French Space Agency CNES and ANR (ANR-19-CE31-0008). PL, ES, ZX acknowledge Idex Paris Cité (ANR-18-IDEX-0001). The research was carried out in part at the Jet Propulsion Laboratory, California Institute of Technology, under a contract with the National Aeronautics and Space Administration (80NM0018D0004). Open access funding enabled and organized by Projetk DEAL. This is InSight contribution ICN 299.

Open Research

The event information of the martian seismic events can be found in the InSight seismic event catalog version 13 (InSight Marsquake Service, 2023). The waveform data and station metadata are available from IPGP's MSDC as well as from IRIS MDC (InSight Mars SEIS Data Service, 2019). Seismic data for station DREG (BQ network, 2016) are publicly available via EIDA (http://eida.gfz-potsdam.de/webdc3/). The GCMT catalog is available here `https://www.globalcmt.org/CMTsearch.html`, whereas the events analyzed for the Earth case and the codes utilized for the processing of the events can be found under `https://github.com/scarrascom/rayleigh_ellipticity`.

References

Ammon, C. J. (1991). The isolation of receiver effects from teleseismic p waveforms. *Bull. Seismol. Soc. Am*, *81*(6), 2504–2510.

Attanayake, J., Ferreira, A. M., Berbellini, A., & Morelli, A. (2017). Crustal structure beneath Portugal from teleseismic Rayleigh Wave Ellipticity. *Tectonophysics*, *712-713*, 344-361. doi: https://doi.org/10.1016/j.tecto.2017.06.001

Banerdt, W., Smrekar, S., Banfield, D., Giardini, D., & et al. (2020). Initial results from the InSight mission on Mars. *Nature Geoscience*, *13*, 183-189. doi: 10.1038/s41561-020-0544-y

Beghein, C., Li, J., Weidner, E., Maguire, R., Wookey, J., Lekić, V., ... Banerdt, W. (2022). Crustal Anisotropy in the Martian lowlands from surface waves. *Geophysical Research Letters*, *49*(24), e2022GL101508.

Berbellini, A., Morelli, A., & Ferreira, A. M. (2016). Ellipticity of Rayleigh waves in basin and hard-rock sites in Northern Italy. *Geophysical Journal International*, *206*(1), 395–407.

Berbellini, A., Morelli, A., & G. Ferreira, A. M. (2017). Crustal structure of northern Italy from the ellipticity of Rayleigh waves. *Physics of the Earth and Planetary Interiors*, *265*, 1-14. Retrieved from `https://www.sciencedirect.com/science/article/pii/S0031920116302412` doi: https://doi.org/10.1016/j.pepi.2016.12.005

BQ network. (2016). *Bensberg Earthquake Network.* International Federation of Digital Seismograph Networks. Retrieved from `https://www.fdsn.org/networks/detail/BQ/` doi: 10.7914/SN/BQ

Carrasco, S., Knapmeyer-Endrun, B., Margerin, L., Schmelzbach, C., Onodera, K., Pan, L., ... Banerdt, W. (2022, 10). Empirical H/V spectral ratios at the InSight landing site and implications for the martian subsurface structure. *Geophysical Journal International*, *232*(2), 1293-1310. Retrieved from `https://doi.org/10.1093/gji/ggac391` doi: 10.1093/gji/ggac391

Chong, J., Ni, S., Chu, R., & Somerville, P. (2016). Joint Inversion of Body-Wave Receiver Function and Rayleigh-Wave Ellipticity. *Bulletin of the Seismological Society of America*, *106*(2), 537–551.

Durán, C., Khan, A., Ceylan, S., Zenhäusern, G., Stähler, S., Clinton, J., & Giardini, D. (2022). Seismology on Mars: An analysis of direct, reflected, and converted seismic body waves with implications for interior structure. *Physics of the Earth and Planetary Interiors*, *325*, 106851. Retrieved from `https://www.sciencedirect.com/science/article/pii/S0031920122000127` doi: https://doi.org/10.1016/j.pepi.2022.106851

Evernden, J. F. (1953). Direction of approach of Rayleigh waves and related problems: (Part I). *Bulletin of the Seismological Society of America*, *43*(4), 335–374.

Ferreira, A. M., Marignier, A., Attanayake, J., Frietsch, M., & Berbellini, A. (2020). Crustal structure of the Azores Archipelago from Rayleigh wave ellipticity data. *Geophysical Journal International*, *221*(2), 1232–1247.

Ferreira, A. M., & Woodhouse, J. H. (2007). Observations of long period Rayleigh wave ellipticity. *Geophysical Journal International*, *169*(1), 161–169.

Heap, M. J. (2019). P-and S-wave velocity of dry, water-saturated, and frozen basalt: Implications for the interpretation of Martian seismic data. *Icarus*, *330*, 11–15.

Hobiger, M., Cornou, C., Wathelet, M., Giulio, G. D., Knapmeyer-Endrun, B., Renalier, F., ... others (2013). Ground structure imaging by inversions of Rayleigh wave ellipticity: sensitivity analysis and application to European strong-motion sites. *Geophysical Journal International*, *192*(1), 207–229.

Hobiger, M., Hallo, M., Schmelzbach, C., Stähler, S., Fäh, D., & et al. (2021). The shallow structure of Mars at the InSight landing site from inversion of ambient vibrations. *Nature Communication*, *12*, 6756. doi: 10.1038/s41467-021-26957-7

InSight Mars SEIS Data Service. (2019). *SEIS raw data, Insight Mission. IPGP, JPL, CNES, ETHZ, ICL, MPS, ISAE-Supaero, LPG, MFSC.* Retrieved from `https://doi.org/10.18715/SEIS.INSIGHT.XB_2016` (10.18715/SEIS.INSIGHT.XB_2016)

InSight Marsquake Service. (2023). *Mars Seismic Catalogue, InSight Mission; V13 2023-01-01 (Version 13.0). ETHZ, IPGP, JPL, ICL, Univ. Bristol.* [dataset]. Retrieved from `https://www.insight.ethz.ch/seismicity/catalog/v13` doi: 10.12686/a19

Ji, C., Tsuboi, S., Komatitsch, D., & Tromp, J. (2005). Rayleigh-wave multipathing along the west coast of North America. *Bulletin of the Seismological Society of America*, *95*(6), 2115–2124.

Joshi, R., Knapmeyer-Endrun, B., Mosegaard, K., Wieczorek, M. A., Igel, H., Christensen, U., & Lognonné, P. H. (2023). Joint Inversion of receiver functions and apparent incidence angles to determine the crustal structure of Mars. *Geophysical Research Letters*, e2022GL100469. Retrieved from `https://doi.org/10.1029/2022GL100469` doi: 10.1029/2022GL100469

Kawamura, T., Clinton, J. F., Zenhäusern, G., Ceylan, S., Horleston, A. C., Dahmen, N. L., ... Banerdt, W. B. (2022). S1222a - the largest Marsquake detected by InSight. *Geophysical Research Letters*, *n/a*(n/a), e2022GL101543. (e2022GL101543 2022GL101543) doi: https://doi.org/10.1029/2022GL101543

Kim, D., Banerdt, W., Ceylan, S., Giardini, D., Lekić, V., Lognonné, P., ... others (2022). Surface waves and crustal structure on Mars. *Science*, *378*(6618), 417–421.

Kim, D., Lekić, V., Irving, J. C., Schmerr, N., Knapmeyer-Endrun, B., Joshi, R., ... others (2021). Improving constraints on planetary interiors with PPS receiver functions. *Journal of Geophysical Research: Planets*, *126*(11), e2021JE006983.

Kim, D., Stähler, S. C., Ceylan, S., Lekic, V., Maguire, R., Zenhäusern, G., ... Banerdt, W. B. (2022). Structure Along the Martian Dichotomy Constrained by Rayleigh and Love Waves and their Overtones. *Geophysical Research Letters*, *n/a*(n/a), e2022GL101666. (e2022GL101666 2022GL101666) doi: https://doi.org/10.1029/2022GL101666

Knapmeyer-Endrun, B., Panning, M., Bissig, F., Joshi, R., Khan, A., D, D. K., ... et al. (2021). Thickness and structure of the martian crust from InSight seismic data. *Science*, *373*(6553), 438-443. doi: 10.1126/science.abf8966

Li, G., Chen, H., Niu, F., Guo, Z., Yang, Y., & Xie, J. (2016). Measurement of Rayleigh wave ellipticity and its application to the joint inversion of high-resolution S wave velocity structure beneath northeast China. *Journal of Geophysical Research: Solid Earth*, *121*(2), 864–880.

Li, J., Beghein, C., Davis, P., Wieczorek, M. A., Mclennan, S. M., Kim, D., ... others (2022). Crustal Structure Constraints from the Detection of the SsPp Phase on Mars. *Earth and Space Science*, e2022EA002416.

Li, J., Beghein, C., Lognonné, P., McLennan, S. M., Wieczorek, M., Panning, M., ...

Banerdt, W. B. (2022). Different Martian Crustal Seismic Velocities across the Dichotomy Boundary from Multi-Orbiting Surface Waves. *Geophysical Research Letters*, e2022GL101243.

Li, J., Beghein, C., McLennan, S. M., Horleston, A. C., Charalambous, C., Huang, Q., ... others (2022). Constraints on the martian crust away from the InSight landing site. *Nature Communications*, *13*(1), 7950.

Li, J., Beghein, C., Wookey, J., Davis, P., Lognonné, P., Schimmel, M., ... Banerdt, W. B. (2022). Evidence for crustal seismic anisotropy at the InSight lander site. *Earth and Planetary Science Letters*, *593*, 117654.

Lin, F.-C., Schmandt, B., & Tsai, V. C. (2012). Joint inversion of rayleigh wave phase velocity and ellipticity using usarray: Constraining velocity and density structure in the upper crust. *Geophysical Research Letters*, *39*(12).

Lognonné, P., Banerdt, W. B., Giardini, D., Pike, W. T., Christensen, U., Laudet, P., ... others (2019). Seis: Insight's seismic experiment for internal structure of mars. *Space Science Reviews*, *215*(1), 1–170.

Lognonné, P., Banerdt, W., Pike, W., Giardini, D., & Zweifel, P. (2020). Constraints on the shallow elastic and anelastic structure of Mars from InSight seismic data. *Nature Geoscience*, *13*(3), 213-220. doi: 10.1038/s41561-020-0536-y

Pan, L., Quantin-Nataf, C., Tauzin, B., Michaut, C., Golombek, M., & Lognonné, P. (2020). Crust stratigraphy and heterogeneities of the first kilometers at the dichotomy boundary in western Elysium Planitia and implications for InSight lander. *Icarus*, *228*, 113511. doi: 10.1016/j.icarus.2019.113511

Panning, M. P., Banerdt, W. B., Beghein, C., Carrasco, S., Ceylan, S., Clinton, J. F., ... Zenhäusern, G. (2022). Locating the largest event observed on mars with multi-orbit surface waves. *Geophysical Research Letters*, *n/a*(n/a), e2022GL101270. (e2022GL101270 2022GL101270) doi: https://doi.org/10.1029/2022GL101270

Panning, M. P., Lognonné, P., Bruce Banerdt, W., Garcia, R., Golombek, M., Kedar, S., ... others (2017). Planned products of the Mars structure service for the InSight mission to Mars. *Space Science Reviews*, *211*(1), 611–650.

Pedersen, H., Boué, P., Poli, P., & Colombi, A. (2015). Arrival angle anomalies of Rayleigh waves observed at a broadband array: a systematic study based on earthquake data, full waveform simulations and noise correlations. *Geophysical Supplements to the Monthly Notices of the Royal Astronomical Society*, *203*(3), 1626–1641.

Posiolova, L. V., Lognonné, P., Banerdt, W. B., Clinton, J., Collins, G. S., Kawamura, T., ... others (2022). Largest recent impact craters on Mars: Orbital imaging and surface seismic co-investigation. *Science*, *378*(6618), 412–417.

Sambridge, M. (1999). Geophysical inversion with a neighbourhood algorithm—I. Searching a parameter space. *Geophysical journal international*, *138*(2), 479–494.

Savitzky, A., & Golay, M. J. (1964). Smoothing and differentiation of data by simplified least squares procedures. *Analytical chemistry*, *36*(8), 1627–1639.

Schimmel, M., Stutzmann, E., Lognonné, P., Compaire, N., Davis, P., Drilleau, M., ... Banerdt, B. (2021). Seismic Noise Autocorrelations on Mars. *Earth and Space Science*, *8*(6), e2021EA001755. (e2021EA001755 2021EA001755) doi: https://doi.org/10.1029/2021EA001755

Sexton, J. L., Rudman, A., & Mead, J. (1977). Ellipticity of Rayleigh waves recorded in the Midwest. *Bulletin of the Seismological Society of America*, *67*(2), 369–382.

Shi, J., Plasman, M., Knapmeyer-Endrun, B., Xu, Z., Kawamura, T., Lognonné, P., ... Wang, T. (2022). High-frequency receiver functions with event S1222a reveal a discontinuity in the Martian shallow crust. *Geophysical Research Letters*, 10.1029/2022GL101627.

Shibutani, T., Sambridge, M., & Kennett, B. (1996). Genetic algorithm inversion

for receiver functions with application to crust and uppermost mantle structure beneath eastern australia. *Geophysical Research Letters*, *23*(14), 1829–1832.

Tanimoto, T., & Rivera, L. (2008). The ZH ratio method for long-period seismic data: sensitivity kernels and observational techniques. *Geophysical Journal International*, *172*(1), 187–198.

Tanuma, K., & Man, C.-S. (2008). Perturbation formulas for polarization ratio and phase shift of Rayleigh waves in prestressed anisotropic media. *Journal of Elasticity*, *92*(1), 1–33.

Warner, N., Golombek, M., Ansan, V., Marteau, E., Williams, N., Grant, J., & et al. (2022). In situ and orbital stratigraphic characterization of the InSight landing site—A type example of a regolith-covered lava plain on Mars. *Journal of Geophysical Research: Planets*, *127*. doi: 10.1029/2022JE007232

Wathelet, M. (2005). Array recordings of ambient vibrations: surface-wave inversion. *PhD Diss., Liége University*, *161*.

Wathelet, M. (2008). An improved neighborhood algorithm: parameter conditions and dynamic scaling. *Geophysical Research Letters*, *35*(L09301). doi: 10.1029/2008GL033256

Wieczorek, M. A., Broquet, A., McLennan, S. M., Rivoldini, A., Golombek, M., Antonangeli, D., ... Banerdt, W. B. (2022). InSight Constraints on the Global Character of the Martian Crust. *Journal of Geophysical Research: Planets*, *127*(5), e2022JE007298. Retrieved from `https://agupubs.onlinelibrary.wiley.com/doi/abs/10.1029/2022JE007298` (e2022JE007298 2022JE007298) doi: https://doi.org/10.1029/2022JE007298

Yano, T., Tanimoto, T., & Rivera, L. (2009). The ZH ratio method for long-period seismic data: inversion for S-wave velocity structure. *Geophysical Journal International*, *179*(1), 413–424.